Kennett, J.P., Baldauf, J.G., and Lyle, M. (Eds.), 1995
Proceedings of the Ocean Drilling Program, Scientific Results, Vol. 146 (Pt. 2)

4. THE ODP COLOR DIGITAL IMAGING SYSTEM: COLOR LOGS OF QUATERNARY SEDIMENTS FROM THE SANTA BARBARA BASIN, SITE 893[1]

Russell B. Merrill[2] and John W. Beck[2]

ABSTRACT

Digital color logs of cores from Leg 146, Holes 893A and 893B, have been taken from images captured during January 1993, within days after the cores were split and described. The images were captured and color analyses performed on the Ocean Drilling Program (ODP) color digital imaging system, which was assembled from relatively inexpensive, off-the-shelf components. The images were used to calculate sedimentation rates by fitting chronological data from Hole 893A to void-corrected depths determined by eliminating all voids mapped from the images as >1 cm in length measured downcore. Color measurements were made at intervals between 0.22 and 1.0 mm in length, and then *Commission Internationale de l'Eclairage* (CIE) 1931 chromaticity values were computed. Results plotted within CIE chromaticity space lie in close proximity to the Munsell 5Y hue plane, confirming that the instrumental color analysis technique has produced results consistent with those of the human observers who described colors visually. Significant periodicities occurring at 12, 17, 31, and 90 years correlate with sunspot activity cycles, suggesting that color variations may reflect global climatic forcing functions. Linear correlation between color data sets from Holes 893A and 893B suggests that as much as 1.2 m of material present at or near the top of Hole 893B may not have been recovered from Hole 893A, and that there is a 70-cm depth discrepancy in the opposite direction at 51.5 meters below seafloor (mbsf). The paper recommends that the 1931 CIE chromaticity system be used routinely for describing colors of geological materials because it readily accommodates the mathematical manipulations required for statistical and time-series analyses and avoids the subjectivity and other weaknesses inherent in the Munsell Color System.

INTRODUCTION

The growing importance of high resolution paleoceanographic studies in recent years has aggravated the need to reconstruct comprehensive, continuous columnar sections from well logs and recovered cores. Ideally, these reconstructions should be completed within a few hours of recovering the cores or obtaining the well log data; however, reality is that reconciling the various depth measurements associated with multiple holes and multiple tools is a major challenge, especially when core recovery is not equal to 100 percent of the drilled interval.

Color is a readily observable physical property, and one which has long been used by geologists to correlate beds visible in outcrop. Unfortunately, the colors of most fresh marine sediments are too ephemeral, and color differences between layers typically are too subtle and too abundant for quantitative work to be accomplished reliably by human inspection. Overcoming these problems would allow the color properties of the sediment column to be studied as proxy records of changes in the climatic, depositional, erosional, and consolidation environments that have affected local events. Readily comparable data sets derived from closely spaced measurements also allow standard correlation techniques to be used to adjust depths between holes and to detect missing intervals for the guidance of the shipboard party during drilling, as well as in subsequent scientific studies.

The Ocean Drilling Program (ODP) color digital imaging system is a candidate instrument for inclusion on a future multi-sensor track (MST) for split core analyses on board the *JOIDES Resolution,* should funds become available for development of such an MST. The system is based entirely upon relatively inexpensive off-the-shelf components, so it can be deployed in any laboratory.

Like the shipboard archival photographs, images captured with the ODP digital imaging system can be used long after the cruise for studies of structures, textures, bioturbation, and other physical aspects of cores visible in the split surface. Unlike archival photographs, in which emulsion dyes often change significantly within a few years of exposure, digital images preserve color information indefinitely, so an ephemeral physical property can now be studied quantitatively during and a cruise and after the cruise is over. Because color can be measured objectively and quantitatively from digital images at any desired interval (minimum size is a single pixel), the system offers data appropriate for a variety of uses. Colors can be measured essentially continuously along the length of a core, providing a dense data set suitable for core-core correlation or time-series analysis, which then can be smoothed for inspection or plotting at spacings comparable with analyses made at discrete intervals, such as sample-derived geochemical parameters or measurements from the whole-core MST. Depending upon the physical condition of the cores and the resulting color data quality, core-core correlations may be performed aboard the vessel in near real-time or may require significant post-cruise processing.

The Munsell Color System, which has been used traditionally to describe sediment colors, is a qualitative system dependent upon visual comparison of sample color chips by observers working under ideal (but rarely achieved) lighting conditions. Data recorded in the Munsell System cannot readily be manipulated or compared mathematically and, inevitably, vary in quality as observers and observational conditions change. These problems have contributed to the difficulty of comparing and using recorded color observations for scientific interpretations. One of the objectives of this study, therefore, has been to evaluate an internationally recognized color classification

[1]Kennett, J.P., Baldauf, J.G., and Lyle, M. (Eds.), 1995. *Proc. ODP, Sci. Results,* 146 (Pt. 2): College Station, TX (Ocean Drilling Program).

[2]Ocean Drilling Program, Texas A&M University Research Park, 1000 Discovery Drive, College Station, TX 77845-9547, U.S.A.

system, the *Commission Internationale de l'Eclairage* (CIE) 1931 chromaticity system, for use in describing geological materials.

This is the first report of an investigation that applies digital video capture and digital still camera technology to the making of quantitative, continuous color measurements of fresh marine sediment cores and to the adjustment of depth scales for drilling and coring artifacts. It also is the first attempt to use the CIE 1931 chromaticity system to record sediment color properties so that they can be manipulated in time-series analyses and correlated with other physical properties measurements. Preliminary results of the study have been described by Rack et al. (1993) and by Rack et al. (1994). This paper describes the ODP color digital imaging system in its role as a color logging tool, along with the application of that tool to Quaternary sediments recovered from the Santa Barbara Basin at Site 893. The color data are correlated with the Site 893 magnetic susceptibility data by Rack and Merrill (this volume).

BACKGROUND

Site 893 is located at 34°17.25′N, 120°02.19′W at a water depth of 576.5 m in the Santa Barbara Basin, approximately 20 km south of Santa Barbara, California. During December 1992 two holes were drilled 10 m apart: 21 cores to a depth of 196.5 m below the seafloor (mbsf) from Hole 893A; 8 APC cores were recovered from Hole 893B, reaching a total depth of 68.8 mbsf. The cores were returned to the Gulf Coast Repository, College Station, Texas, without being split.

The scientific party met at the Repository during January 1993 to split, describe, and sample the cores. Sediments recovered from Site 893 consist largely of clays, silty clays, and sands intermixed with biogenic material (carbonate and opal). See Kennett, Baldauf, et al. (1994) for a complete description.

Color Measurement

Colors have always been recognized as important properties of natural materials, including rocks and soils. Color differences are among the most easily observed physical properties, but because they are difficult to describe unambiguously and comprehensibly to others, few geologists have attempted quantitative studies. Clearly, it would be desirable to be able to study color differences quantitatively, like other physical properties, in order to use them as guides to sedimentary processes and as keys to intercore depth correlation.

A number of systems have been devised for describing colors of materials by comparing them to widely distributed sets of color chips (Wyszecki and Stiles, 1982). Of these, the Munsell Color System has become widely accepted by geologists and has been employed in describing Deep Sea Drilling Project (DSDP) and ODP cores since the beginning of the drilling program. The Munsell Color System is based upon the work of Albert H. Munsell (1929, 1963; Billmeyer and Saltzman, 1981), who assembled a collection of color samples believed to represent equal intervals of visual perception and devised a three-coordinate system (hue, value, chroma) to describe all possible colors. Munsell hue is expressed by a combination of numbers and letters (e.g., 2.5Y) which describes a color's property of being Yellow, Red, Green, Blue, Purple or binary mixtures thereof. Munsell value describes the color's lightness relative to a gray scale ranging from white to black, while Munsell chroma corresponds to the degree of difference between a color (other than black, white or gray) and a gray of the same value or lightness. Within the Munsell System, therefore, a red-brown might be described as 5YR 5/6, where 5YR is the hue, 5/ is the value, and /6 is the chroma.

The color-measurement tool traditionally employed on board the drilling vessel has been a 5- × 8-inch notebook, *Munsell Soil Color Charts* (Munsell Color, Macbeth Division, Kollmorgen Corporation, Baltimore, MD, U.S.A.), containing 12 charts and 300 color chips, from which scientists describing cores attempt to select the closest match or to interpolate values. The system is simple to use, easily comprehensible, and requires minimal training. Unfortunately, measurements are labor-intensive, hard to replicate, and difficult to manipulate mathematically.

Practical difficulties in applying the Munsell technique (or similar chip comparison systems) include variability in observers' color perceptions; lighting (the Munsell Color System requires that the illumination be daylight balanced, whereas the description table aboard the *JOIDES Resolution* is lit with cool-white fluorescent lamps); and alteration of the color reference chips due to age, handling, and exposure to mud and water. Generally, sediment colors observed on the description table are ephemeral, changing rapidly as the surface of the split core oxidizes, so it is difficult to reproduce a color observation only hours after making it, even if the same set of color chips can be employed.

If the observational difficulties in applying the Munsell Color System to deep-sea sediment cores could be overcome, then we must deal with the fact that the system does not describe colors in a physical continuum, but only in terms of members of a physical set of color chips. Sediment samples that appear to match members of the chip set almost certainly contain coloring agents with spectral characteristics different from those of the chip (i.e., the sediment and the chip form a metameric pair), so the match is valid only under the precise conditions of the original observation, including the color temperature of the lights and the identity of the observer.

Inherently, comparison-based color description systems like Munsell cannot provide quantitative data of the quality produced, for example, by the magnetic susceptibility, *P*-wave, GRAPE, Hamilton vane shear, or other physical properties instruments routinely used on board ship.

CIE Color Space

The group that sets the standards for measuring and describing color is the *Commission Internationale de l'Eclairage.* This commission has established a number of applicable standards, the choice of which depends upon the precise nature of the measurement and conditions of observation. The standards appropriate for use with the ODP digital imaging system are the CIE 1931 Standard Colorimetric Observer, CIE Standard Sources D (Daylight Simulators), and CIE 1931 Standard Colorimetric System (Wyszecki and Stiles, 1982), which will be employed throughout this paper.

CIE 1931 chromaticity (x, y, Y) space is illustrated in Figure 1. This three-dimensional shape bounds the region of observable colors within CIE tristimulus space. Within CIE chromaticity space, colors are described uniquely and continuously in terms of the three coordinates x, y, and z. These dimensions are related to the CIE primary tristimulus values (X, Y, Z) as follows:

$$x = \frac{X}{(X+Y+Z)},$$

$$y = \frac{Y}{(X+Y+Z)},$$

$$z = \frac{Z}{(X+Y+Z)}.$$

Because these coordinates sum to 1, a tristimulus value, usually Y, must also be specified to define each color uniquely. By convention, Y is plotted perpendicular to the x, y-surface (parallel to the z-axis) and is thought of as defining the luminance of the color.

Intuitively, luminance (Y) is analogous to value in the Munsell System or to brightness (a perfect white reflector would have Y = 100), while the (x, y) coordinates describe the other properties of a color, which are in some degree analogous to Munsell hue and chro-

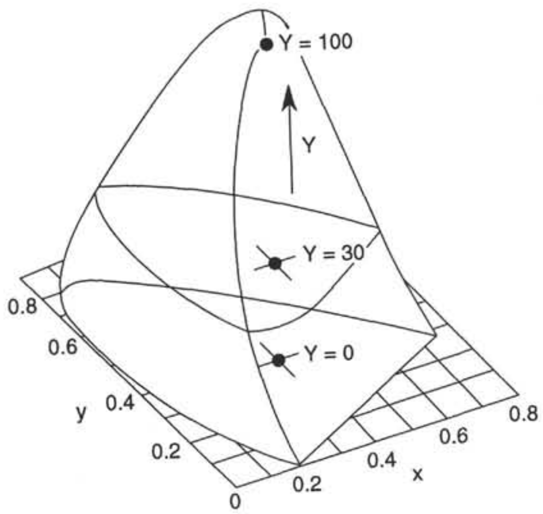

Figure 1. CIE 1931 chromaticity (x, y, Y) space located within CIE tristimulus (X, Y, Z) space. Modified after Agoston (1987).

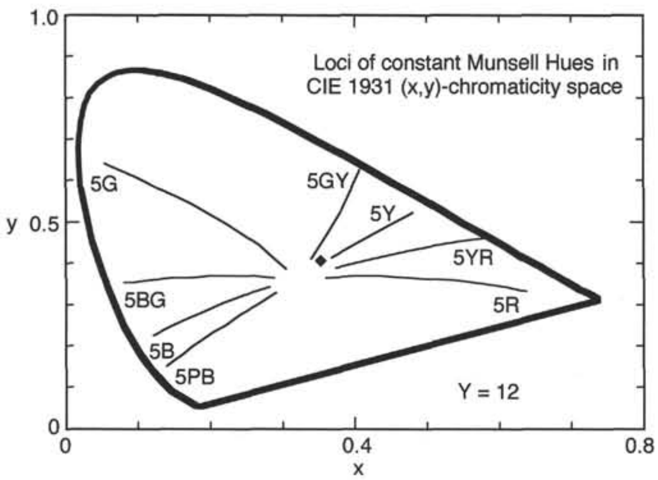

Figure 2. Projection of Munsell hues into the CIE (x, y) chromaticity coordinate plane. Heavy line envelopes base of the three-dimensional (x, y, Y) shape seen in Figure 1. Munsell hues occupy surfaces within this shape, locations of which were determined empirically by Newhall et al. (1943). Filled diamond marks location of the D_{5000} light source employed in this study.

ma. For reference, Munsell hue surfaces are projected onto the (x, y) chromaticity plane in Figure 2. Very simplistically, increasing values of y correlate with increasing yellow content, while x ranges between blue and red.

The clear advantages that the CIE chromaticity system offers over the Munsell System are that effects of changing illuminants and/or observers are calculable so measurements are easily verifiable and reproducible with different instruments, and normal mathematical relationships apply so that statistical manipulations are valid.

There is no free lunch, of course. The principal drawback of the CIE chromaticity system is that it distorts some regions of color space, much as a Mercator projection distorts portions of a map remote from its center. This distortion is irrelevant to most geological applications, but there are some awkward moments. For example, all three tristimulus values (X, Y, Z) of the color black equal zero by definition so true black lies anywhere and everywhere in the x, y-plane (z, Y = 0) of the chromaticity diagram. Colors close to black can be difficult to characterize uniquely. Coal geologists may wish to avoid ambiguity by selecting a coordinate system with more emphasis on shades of gray and black, but most geologists will be well served by the CIE chromaticity system.

Instruments

Four instrument systems capable of making color measurements have been employed on ODP cores recently: a multi-wavelength scanner (Leg 138; Mix et al., 1992), a Minolta CM-2002 color scanner (Leg 145; Rea et al., 1993), an OptoTech color digitizer (Schaaf and Thurow, in press; see also Schaaf and Thurow, this volume), and the ODP color digital imaging system (Leg 146; Kennett, Baldauf, et al., 1994), which is the subject of this paper. The prototype multi-wavelength scanner deployed on Leg 138 measured reflectance at 511 different wavelengths from a 2-cm-wide spot centered in the split core. The normal interval between measurements was 4 cm, which proved adequate for correlating depths among adjacent holes. The large number of wavelengths measured extends the capability of this instrument well beyond color measurement, enabling users to distinguish lithologic components by differential reflectance (Mix et al., 1995). The authors reported results in terms of relative reflectances in red, green, and blue portions of the spectrum rather than in terms of color, but it should be straightforward to compute color values from their data if calibration procedures were followed.

The Minolta scanner, which now is routinely available on the *JOIDES Resolution,* is a computer peripheral that resembles a gun that can be aimed at a target of interest and triggered to report color reflectance (31 wavelength channels between 400 and 700 nm) in various standard formats, including Munsell and CIE chromaticity. The output of the instrument can be directed to an IBM PC-clone for capture.

The OptoTech 8-bit color scanner (described by Schaaf and Thurow, in press) requires three passes over the target core, each with a different filter, in order to capture three monochrome images which then are merged to form a 24-bit color image. This device would be at a disadvantage aboard the ship because of vibration; however, it is appropriate for use on shore. Schaaf and Thurow (this volume) have used this instrument to capture 8-bit images of the Site 893 cores in shades of gray.

ODP Digital Imaging System

The imaging system consists of four components: lights, cameras, computers, and software. Cores or samples to be imaged are placed on an illuminated copy stand so that an image can be formed within either a video camera or a digital still camera. The image is captured with a microcomputer, and then stored on archival media. Images can be processed later with a variety of image processing packages, including the ODP color measurement software discussed in this paper. All electronic components are available off-the-shelf. Satisfactory substitutes are available from these and other manufacturers at a wide variety of costs, depending upon the resolution and accuracy required.

The geometry of lights and camera (Fig. 3) conform to the CIE 45/0 standard for viewing and illumination.

Cameras

The ODP digital imaging system is equipped with two cameras:

1. A SONY DXC-750MD NTSC camera equipped with three CCDs (768 × 493 array) and a Fujinon TV.Z 4 × 7.5 lens. This camera is preferred for imaging on board a ship because it delivers the red (centered at 700 nm), green (546 nm), and blue (436 nm) images simultaneously, reducing the chance that vibration will adversely affect registration of the images. SONY declines to publish more detailed information on wavelength

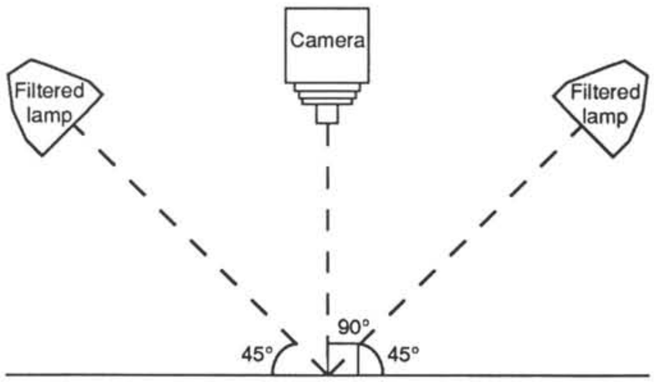

Figure 3. Geometry of the ODP digital imaging system complies with CIE (45/0) conditions for illumination and viewing. Video or digital still camera feeds image to a PC-clone or to a Macintosh microcomputer, where it is processed and archived.

sensitivity; however, it is available to customers who sign a nondisclosure agreement.

2. A LEAF (Southboro, MA) digital still-camera back, mounted on a Hasselblad ELX camera body equipped with a Hasselblad 50mm Distagon lens, is used to capture close-up images on shore. This camera, which has a digital resolution of 2048 × 2048 42-bit pixels, employs a filter-wheel to generate red, blue, and green images sequentially. The filters are Kodak Wratten #25, #58, and #47B. Detailed filter specifications are reported in Kodak (1990).

Illumination

Illumination for the SONY video camera version of the system consists of two tungsten lamps filtered to a color temperature of 5020°K. The color temperature of light incident on the core samples ranges between 4300°K and 4600°K, with variations resulting primarily from the aging of bulbs. Tungsten bulbs age rapidly, with significant color temperature variations observable within hours. Some variation in color temperature can be accommodated by frequent recalibration (in this study, calibration images were captured between every section of core); however, the difficulty of finding stable, daylight-color-balanced lighting sources is a real problem for this kind of work. Most commercially available lights are designed for film photography, which is more tolerant of lighting variations than is colorimetry.

UV-corrected, daylight-balanced strobes (5500°K) are used to illuminate the copy stand when the LEAF digital still camera is installed. Strobes are much less prone to change color temperature with age than are the tungsten bulbs.

If desired, data sets can be corrected for nonuniform light distribution by fitting curves independently to each channel of color intensity data derived from a uniform surface, such as an unexposed photographic emulsion. These curves can then be ratioed with data derived from samples in order to accomplish the correction. Data reported in this paper were not corrected for the effects of nonuniform light distribution because the magnitude of such corrections was observed to be less than noise.

Computers

The SONY video camera is supported by a Truevision (Indianapolis, IN) AT-Vista 4-Mb video capture board equipped with a 10-Mb AT/VMX auxiliary memory board and mounted in an IBM 486/DX66 clone. As of this writing, Truevision has merged with RasterOps (Santa Clara, CA). The LEAF digital camera back is supported by a Macintosh Quadra 800 equipped with a RasterOps 8/24XLi video board.

Captured images are stored in extended TGA (TGA 2.0) format on magnetic or magneto-optical discs for immediate use, and on 4-mm DAT tape or ISO-9660 CD-R discs for archival storage. Digital images can be extremely large: images produced by the SONY camera system may be as large as 3 Mb, and those produced by the LEAF camera are 26 Mb each. LEAF images are stored in 48-bit TIFF 6.0 format initially, but are transformed to 24-bit TGA 2.0 images for use with the ODP color measurement system.

Computer Software

The ODP Color Measurement software, which supports digital image capture and color analysis on the 486 clone, is written in Microsoft C and Fortran, and makes use of proprietary libraries written by Truevision and IMSL. Details of algorithms are available from the authors if desired. Images from the LEAF camera are captured with proprietary software from LEAF, and are then converted to TGA 2.0 formats in ADOBE Photoshop.

Core images used for most of this study were captured with the SONY DXC-750MD camera and the Truevision AT-Vista capture board operating at a resolution of 1008 × 486 16-bit pixels, with 5 bits of color information allocated to each channel. At this resolution, the system can distinguish 32,768 different colors; however, quantization effects are observable in data from areas with similar colors. It would have been better to use 24-bit pixels, but storage logistics precluded this option at the time. The LEAF camera was used to capture high-resolution images used in fine-scale correlation.

METHODS

During the post-Leg 146 sampling party of January 1993, cores from Site 893 were split, scraped gently with a razor blade to remove surface disturbances, and imaged. Using the SONY video camera, a 1008 × 486-pixel 16-bit color image was captured of each 10-cm interval of the split core, overlapping at both ends of each interval so that each image covers a 13.5-cm length of core. Each pixel spans about 134 µm along the length of the core and 210 µm along the diameter. The image capture process was not automated, so approximately two weeks were required to complete the task. Because of this delay, it was impossible to image all of the cores while perfectly fresh, so all surfaces were allowed to oxidize prior to imaging.

Images of color calibration standards were captured between every core section in order to minimize possible effects of drifting illuminant color temperatures caused by aging tungsten lamps. Primary calibration standard was a set of red, green, blue, white, and gray color chips supplied by MacBeth (Kollmorgen Corporation, Baltimore, MD), supplemented by the Kodak Color Separation Guide and Gray Scale (CAT 1527654). Images of 12 British Ceramic Research Association (BCRA) Ceramic Color Standards, calibrated by the Hemmendinger Color lab (Princeton, NJ), were captured at less frequent intervals to ensure that the primary color standards remained stable. All standards remained stable throughout the period of image capture.

Using the ODP color system (v. 1.1) software, color measurements were made at 1-mm intervals downcore through all images of Hole 893B cores and through all images of Hole 893A, Cores 1H and 4H–11H. Measurements were made at 0.6-mm intervals downcore through all images of Hole 893A, Cores 2H, 3H, and 12H–21H. At each individual point, the red, green, and blue values were measured for each pixel in a 9-pixel kernel centered on the measurement point. Pixels that differed from the mean value of their respective color channel by more than one standard deviation were abandoned in order to improve discrimination against edges of the abundant voids and cracks, and adjusted means were calculated from remaining values. The adjusted means were recorded as the red, green and blue (RGB) values of that point.

Using a print of each digital image as a guide, the data were edited to remove points attributable to voids, scrape marks, drilling disturbances, and similar problems. Measurements from the "orphan" sections (pieces recovered from the catwalk after they had been ejected by gas pressure when the cores were first cut) were included only if the sections were in excellent condition, because physical disturbance seriously perturbs color measurements. Depths were closed up only in the case of the voids listed in Table 1; otherwise, bad data points were eliminated without shortening the depth scale, so the color data are compatible with other physical property data compiled on the void-corrected depth scale. Gaps due to the elimination of bad data points were filled by linear interpolation before analyzing the data set as a time series.

RGB values were converted to CIE tristimulus (XYZ) values via the following relationship (Rogers, 1985):

$$\begin{bmatrix} X \\ Y \\ Z \end{bmatrix} = \begin{bmatrix} x_rC_r & x_gC_g & x_bC_b \\ y_rC_r & y_gC_g & y_bC_b \\ (1-x_r-y_r)C_r & (1-x_g-y_g)C_g & (1-x_b-y_b)C_b \end{bmatrix} \begin{bmatrix} R \\ G \\ B \end{bmatrix}$$

where (x_r, y_r), (x_g, y_g), and (x_b, y_b) are CIE chromaticity coordinates for the red, green, and blue channels (primaries) of the camera, respectively. The primary chromaticity coordinates may be available from the manufacturer for some cameras; however, they and the coefficients (C_r, C_g, C_b) remain constant for a given image or set of images, so they can be calculated from measurements of known color standards, which was the procedure followed here. Because images of the standards were captured between every core section, any changes which may have occurred in the optical path or minor variations in illumination are accounted for in the coefficients. Tristimulus values were then converted to CIE chromaticity coordinates (x, y, Y) as discussed earlier.

RESULTS

Final versions of the color data sets for Holes 893A and 893B (Appendix) will be found in spreadsheets, stored as tab-delimited text files suitable for import into Kaleidagraph, located on this volume's CD-ROM.

Because the color digital images are high-resolution maps of the cores, their first application was in locating all voids greater than 1 cm in length downcore, so that the voids could be eliminated from depth calculations made by the entire shipboard party. Using the ODP digital imaging system, each void gap was measured to the nearest 0.5 mm. Preliminary versions of the resulting void catalog and revised top-of-section depths were prepared by Merrill and Rack (Kennett, Baldauf, et al., 1994). Corrected versions are included here as Tables 1 and 2. These tables were made available to all investigators who have contributed to this volume. Additionally, void-corrected depths of all Hole 893A and 893B samples and ages of Hole 893A samples (based on the work of Ingram and Kennett, this volume) were calculated and supplied to these investigators so that analytical results could be plotted on a common scale. Relevant age-depth tie points, resulting curve-fit parameters, and corresponding sedimentation rates are listed in Table 3.

CIE chromaticity data for Holes 893A and 893B are shown in Figure 4, projected into the (x, y) plane, and are projected into the orthogonal (x, Y) and (y, Y) planes in Figures 5 and 6. It is immediately reassuring to note the close agreement between these data and those recorded in the barrel sheets by the sedimentologists who described the major lithologies in the freshly split cores as ranging in color from Munsell 5Y 3/1 to 5Y 6/3, with the majority in the neighborhood of 5Y 4/2 (Kennett, Baldauf, et al., 1994). We get color values from the digital measurements that agree with those we get by visual inspection. It is also pleasing that the digital measurements found colors that are only slightly darker (displaced to lower Munsell values) than those observed in freshly split cores, given the inevitable delay of several days between description and image capture. Oxidation of core surfaces during this period appears to have had little effect upon the digital color measurements.

The data from Holes 893A and 893B are in general agreement; however, there is a noteworthy "tail" observed in the (x, y) data for Hole 893B that is not present in the Hole 893A data. Points in this tail extend parallel to the 5Y 3/ line (Fig. 4) at luminance values (Fig. 6) which are consistently lower than the remainder of the 893B or 893A core. The tail is entirely made up of measurements made at depths shallower than 11.5 mbsf. This tail may reflect different water contents, different oxidation levels, or other geochemical gradients characteristic of sediments near the mud line, but none of these mechanisms explains why the tail is seen in Hole 893B but not in Hole 893A.

Figures 7 and 8 show the chromaticity data from Holes 893A and 893B, respectively, plotted against depth below seafloor corrected by the removal of voids per Table 1. Relatively low values of luminance (Y) are seen to be typical of turbidite sequences, as might be expected because the coarse, granular textures of turbidite intervals absorb light; however, the relationship has not been quantified. A vertical black bar parallel to the Hole 893A luminance plot in Figure 7 marks the interval of the thick turbidite between 113.9 and 116.7 mbsf.

A vertical dashed bar within the Hole 893A y-chromaticity plot (Fig. 7) parallels Core 16H, which is enlarged in Figure 9. Within the first three sections, thin, light olive gray beds intercalated with dark olive gray beds are clearly visible in the archival photograph (Fig. 10). These intercalated light and dark beds appear in the color data (Fig. 9) as peaks of increased luminance correlated with decreased (x, y)-chromaticity. Lower in the core, intercalated beds give way to more massive, structureless sediment that is considerably less variable in color. At the scale at which these data (one point per 0.5 cm) are plotted, the intercalated beds can be mapped easily, and the changing lithology is clearly visible.

Power Spectra

Using linear interpolation, a continuous data set for Hole 893A, Cores 1H–5H, was extracted from the edited but unaveraged color data set and correlated with the age data of Ingram and Kennett (this volume) to yield a time series data set with x, y, Y values every 0.2 years. Power spectra derived from this data set, which contained 144,660 sets of values ranging in age from 30 years to 30,000 years, are shown in Figure 11.

Numerous peaks appear in all three spectra with prominent examples at 12, 17, 31, and 90 years. It is noteworthy that cyclical variations in one coordinate are not always matched by variations in the other two coordinates. For example, there is a moderate peak in the Y data at 23 years which is arguably missing from the x and y spectra, while the prominent peak which appears in the Y data between the 90 and 138 year peaks is much less visible in y and is almost completely missing from the x spectrum. Clearly, factors which affect sediment colors operate independently of one another and are reflected differently by the individual CIE chromaticity coordinates.

Peak positions common to the three spectra agree approximately with reported solar sunspot activity cycles (Landscheidt, 1987) at 11, 22, 31, and 86 years, which indicates that colors of sediments of the Santa Barbara Basin respond to high frequency global climatic forcing functions. This contrasts with the observation of Gardner and

Table 1. Catalog of voids greater than 1 cm observed in digital images of cores from Site 893.

Top of void within section (cm)	Top of void (mbsf)	Void length (cm)
146-893A-		
1H-4, 120.5	5.70	1.5
2H-1, 13.4	6.63	1.5
2H-2, 71.3	8.73	4.3
2H-3, 33.5	9.84	2.7
2H-3, 120	10.70	3.3
2H-3, 141.3	10.92	2.1
2H-4, 15.3	11.16	2.3
2H-4, 35.7	11.36	2.2
2H-4, 49.8	11.50	2.3
2H-4, 81.4	11.82	2
2H-4, 96.1	11.96	5.3
2H-5, 8.6	12.58	5.3
2H-5, 23.8	12.74	1.9
2H-5, 56.5	13.06	4.7
2H-5, 64.2	13.14	2.2
2H-5, 73.6	13.23	1.3
2H-5, 103.9	13.54	2.8
2H-5, 124.1	13.74	1.8
2H-5, 142.9	13.93	2.6
2H-6, 25.8	14.25	3.1
2H-6, 38.4	14.38	2.2
2H-6, 65.5	14.65	1
3H-1, 46.8	16.47	2.7
3H-3, 79	19.78	3.1
3H-3, 90.1	19.89	1
3H-4, 139.3	21.88	5.4
3H-5, 35	22.33	2.4
3H-5, 62	22.60	1.8
3H-5, 67.4	22.65	2.1
3H-5, 76.6	22.74	7.4
3H-6, 20.9	23.68	4.7
4H-1, 62.5	26.13	21.7
4H-1, 85.5	26.36	1.3
4H-2, 22.6	27.21	3.9
4H-2, 50.6	27.49	1.5
4H-2, 124.9	28.24	4.5
4H-3, 70	29.19	2.2
4H-3, 97.1	29.46	3.3
4H-3, 108.8	29.58	2.3
4H-4, 39.8	30.38	2.9
4H-4, 61.8	30.60	9.1
4H-4, 88	30.86	2.7
4H-4, 104.9	31.03	2
4H-4, 130.4	31.29	8.9
4H-5, 69.5	32.18	3
4H-5, 80.1	32.29	2.9
4H-5, 108.6	32.57	1.1
4H-5, 113.8	32.62	1.1
4H-5, 116	32.65	1.4
4H-6, 16	33.13	1
4H-6, 68.8	33.66	1.2
4H-6, 106.9	34.04	2.3
4H-6, 128.5	34.26	2.8
4H-7, 6.7	34.55	4
5H-1, 99.5	36.00	3.6
5H-1, 108.3	36.08	7.5
5H-1, 120.1	36.20	2.5
5H-2, 3.7	36.53	2.2
5H-2, 18.2	36.67	3.6
5H-2, 29.6	36.78	7.6
5H-3, 76.4	38.72	4.6
5H-3, 91.5	38.87	2.3
5H-3, 110.7	39.06	2.4
5H-4, 11	39.55	3.7
5H-4, 17.6	39.61	5
5H-4, 88.5	40.32	3.9
5H-4, 122.3	40.66	2.1
5H-5, 32.4	41.24	1.9
5H-6, 23.8	42.63	3.4
5H-6, 33.7	42.73	2.2
5H-6, 47.2	42.86	1.5
5H-6, 51.7	42.91	1
5H-6, 69.9	43.Q9	2.2
5H-6, 82.3	43.22	6.2
5H-6, 97.5	43.37	6.8
5H-6, 139.3	43.79	5.4
6H-1, 2.7	44.53	2.5
6H-1, 21.2	44.71	4.4
6H-1, 43.8	44.94	9.5
6H-1, 70.5	45.21	2.9
6H-1, 97.8	45.48	15
6H-2, 10.9	46.09	11.5
6H-2, 31.5	46.30	5.3
6H-2, 104.8	47.03	3.8
6H-2, 126.8	47.25	2.2
6H-3, 68.7	48.16	3.6
6H-3, 85.4	48.32	1.1
6H-3, 115.8	48.63	9.7
6H-4, 22.1	49.18	1.8
6H-4, 55.8	49.51	3.4
6H-5, 20.5	50.64	1.7
6H-6, 52.9	52.44	4.9
6H-6, 78.4	52.70	4.4
6H-6, 90.7	52.82	3.7
7H-2, 50.2	54.55	19.5
7H-2, 78.1	54.83	13.2
7H-2, 96.2	55.01	10.5
7H-3, 7.1	55.61	1.6
7H-3, 21.1	55.75	4.1
7H-3, 52.2	56.06	2.9
7H-3, 67.3	56.21	6.4
7H-3, 102.4	56.56	9
7H-3, 123.6	56.78	7.6
7H-3, 134.3	56.88	2.8
7H-4, 0	57.01	5.8
7H-4, 30.3	57.31	3.4
7H-4, 43	57.44	4.5
7H-4, 67.9	57.68	6.5
7H-4, 92.6	57.93	3.9
7H-6, 0	60.05	2.7
7H-8, 41.1	63.41	4.9
8H-2, 135.2	65.00	2.6
8H-2, 139.5	65.05	3.7
8H-3, 7.5	65.22	7.3
8H-3, 37.5	65.52	5.9
8H-3, 44.2	65.59	6.2
8H-3, 85.1	66.00	14.9
8H-3, 109.4	66.24	6.3
8H-3, 126.1	66.41	1
8H-3, 135.2	66.50	4.8
8H-3, 141.2	66.56	3.3
8H-4, 11.9	66.75	6.2
8H-4, 21.9	66.85	6.3
8H-4, 37.9	67.01	10.1
8H-4, 96.3	67.59	2.4
8H-4, 116	67.79	2.4
8H-4, 130.9	67.94	1.9
8H-5, 118.7	69.26	3.5
8H-6, 79.6	70.36	5.3
8H-6, 128.5	70.85	4.1
8H-7, 5.4	71.11	3.4
8H-7, 10.7	71.16	3.2
8H-7, 28.3	71.34	4.5
8H-7, 52.6	71.58	3
8H-7, 118.7	72.24	6.6
8H-8, 4.2	72.66	4.4
8H-8, 12.4	72.66	4.4
8H-8, 36.1	72.90	7.3
8H-8, 65.4	73.19	4.1
9H-1, 60.5	73.61	12.1
9H-1, 75.2	73.75	2.8
9H-1, 116.1	74.16	2.7
9H-1, 128.1	74.28	2.8
9H-1, 134.9	74.35	2.3
9H-2, 37	74.85	3.3
9H-2, 82.2	75.30	4.6
9H-2, 88.9	75.36	1.6
9H-2, 100.8	75.48	4.7
9H-2, 112.7	75.60	3.7
9H-3, 11.5	76.07	4.8
9H-3, 20.3	76.16	2
9H-3, 24.4	76.20	4.6
9H-3, 33.2	76.29	1.2
9H-3, 58.8	76.55	2.3
9H-3, 66	76.62	1.7
9H-3, 80.1	76.76	4.1
9H-3, 92	76.88	4.3
9H-4, 12.4	77.56	1.8
9H-4, 20.6	77.64	2
9H-4, 48.7	77.92	2.1
9H-4, 100.6	78.44	2.7
9H-4, 120.5	78.64	2
9H-4, 128.3	78.72	2.7
9H-5, 60.5	79.53	1.1
9H-7, 5.4	80.59	1.3
9H-7, 17.3	80.71	1.3
9H-7, 19.5	80.73	1.3
9H-7, 31.8	80.86	1
9H-7, 73.2	81.27	0.8
9H-7, 90.3	81.44	4.2
10H-1, 0	82.50	3.1
10H-1, 102.7	83.53	4.3
10H-1, 129.5	83.80	4
10H-2, 36.1	84.35	1.2
10H-4, 93.4	86.49	1
10H-6, 20.4	88.74	2.2
10H-7, 35.6	89.70	2

Table 1 (continued).

Top of void within section (cm)	Top of void (mbsf)	Void length (cm)
11H-1, 0	92.00	1.6
11H-1, 81.2	92.81	2.5
11H-1, 97.4	92.97	5.6
11H-4, 35.5	96.81	5.8
11H-4, 102.7	97.49	4.8
11H-4, 111.9	97.58	8.8
12H-1, 46	101.96	10.7
12H-1, 120.2	102.70	5.8
12H-2, 49.8	103.49	3.3
12H-2, 84.5	103.84	5.8
12H-2, 98	103.97	1
12H-3, 20.2	104.76	2.9
12H-4, 45.9	106.51	5.8
12H-4, 87.3	106.93	2.5
12H-6, 72.8	108.73	4.6
12H-6, 84.3	108.85	1.3
12H-6, 88.2	108.89	9.4
12H-7, 20.3	109.70	1.1
13H-1, 19.1	111.19	14.1
13H-1, 37.1	111.37	1
13H-1, 43.8	111.44	11
13H-1, 95.9	111.96	4.6
13H-3, 117.1	113.84	1.1
13H-4, 0	114.16	17.2
13H-4, 29.1	114.45	1.3
13H-8, 34.9	120.47	9.7
14H-1, 104.2	121.54	3.4
14H-8, 32.2	128.77	1.7
14H-8, 43.5	128.88	1.5
14H-8, 79.8	129.24	1.3
15H-1, 38.4	130.38	27.6
15H-1, 75.8	130.76	1
15H-2, 28.7	131.78	1.1
16H-1, 14.4	139.64	4.4
16H-1, 21.9	139.72	2
16H-1, 32.3	139.82	5.7
16H-1, 50.3	140.00	1.4
16H-1, 87.3	140.37	8.6
16H-1, 113	140.63	3.1
16H-1, 134.3	140.84	5.4
16H-2, 117.8	142.18	1.5
17H-1, 7.9	149.08	1
17H-1, 9.8	149.10	1.3
17H-3, 79.8	152.82	3.5
17H-6, 84.5	157.51	1.1
17H-6, 86.2	157.52	2.2
17H-6, 95.7	157.62	1.1
18H-1, 54.3	158.55	4.9
18H-2, 23.3	160.23	4.5
18H-4, 45.2	163.53	5.2
18H-5, 57.7	165.15	1.5
18H-5, 68.9	165.26	1.1
18H-5, 143.3	166.01	1
18H-6, 25.7	166.31	1.5
18H-6, 105.8	167.12	1.6
18H-6, 110.1	167.16	3.3
18H-7, 12.2	167.69	5.8
19H-1, 10.8	168.11	1
19H-1, 15.4	168.15	1.5
19H-2, 4.5	169.56	1.3
19H-2, 11.8	169.63	4.8
19H-2, 42.1	169.93	1.4
19H-3, 28	171.26	1.2
19H-3, 80.3	171.79	1.4
19H-5, 135.8	175.37	1
19H-6, 83.7	176.34	2.9
20H-1, 11.7	177.62	1.1
20H-1, 28	177.78	4.7
20H-1, 110.9	178.61	1.3
20H-1, 117.7	178.68	9.5
20H-3, 41.3	182.41	7.1
20H-6, 103.3	187.52	1
20H-6, 116.3	187.65	2.1
20H-6, 124.7	187.73	1.3
21H-1, 7.6	187.08	15.4
21H-1, 103.9	188.04	2
21H-2, 36.2	188.46	5.2
21H-2, 148.8	189.58	0.6
21H-3, 41.7	190.20	1.7
146-893B-		
1H-1, 65.9	0.66	5.4
1H-CC, 7.3	2.19	1
2H-1, 0.0	2.30	7.7
2H-4, 36.3	7.22	1
3H-1, 5.7	11.86	4.2
3H-1, 81.8	12.62	6.9
3H-1, 138.8	13.19	5.2
3H-3, 114.3	15.61	3.8
3H-4, 83.3	17.12	4.9
3H-4, 97.5	17.26	1.8
3H-4, 145.5	17.74	2.2
3H-5, 10.8	17.89	2.8
3H-5, 31.4	18.09	2.7
3H-5, 49.0	18.27	2.8
3H-5, 54.6	18.32	1.2
3H-5, 61.7	18.39	2.5
3H-5, 79.2	18.57	6.3
3H-5, 93.9	18.72	9.8
3H-5, 114.9	18.93	7.8
3H-5, 130.6	19.08	3.6
3H-5, 141.2	19.19	3.9
3H-6, 19.1	19.45	6.4
3H-6, 53.0	19.79	9.1
3H-7, 16.3	20.92	1.1
4H-2, 103.4	23.83	1.7
4H-2, 120.8	24.00	2.4
4H-3, 127.2	25.57	1.5
4H-3, 130.9	25.60	1.1
4H-3, 145.8	25.75	1.2
4H-4, 23.4	26.02	2.6
4H-4, 53.7	26.32	1
4H-4, 98.8	26.77	6.3
4H-5, 54.9	27.83	3.4
4H-5, 87.5	28.15	0.8
4H-6, 6.6	28.84	4
4H-6, 18.4	28.96	1.4
4H-6, 146.3	30.24	2.4
4H-7, 7.4	30.35	1.1
4H-7, 18.5	30.46	4.8
5H-1, 65.1	31.45	11.4
5H-1, 99.0	31.79	21
5H-1, 122.6	32.03	1.4
5H-2, 3.4	32.34	1.8
5H-2, 28.1	32.59	1.6
5H-2, 49.5	32.80	7.5
5H-2, 62.7	32.94	9.1
5H-2, 73.2	33.04	1.8
5H-3, 52.1	34.33	1.4
5H-3, 133.3	35.14	1.8
5H-3, 135.7	35.16	1.3
5H-4, 55.5	35.85	3.7
5H-4, 85.5	36.15	7.1
5H-4, 95.9	36.25	6.6
5H-4, 119.8	36.49	1.1
5H-5, 19.6	36.98	5.7
5H-5, 61.5	37.40	2.6
5H-5, 101.6	37.80	4.8
5H-6, 24.1	38.52	2.3
5H-6, 60.2	38.88	3
5H-6, 109.4	39.37	5.3
5H-7, 27.6	40.03	1.4
6H-3, 34.3	43.64	1.8
6H-3, 80.3	44.10	11.9
6H-3, 98.6	44.29	8.1
6H-3, 124.3	44.54	2.3
6H-3, 139.8	44.70	2.4
6H-4, 18.3	44.97	1.1
6H-4, 28.3	45.07	1.2
6H-5, 21.5	46.49	3.6
6H-5, 27.9	46.56	1.3
6H-7, 12.3	49.39	2.4
6H-7, 23.3	49.50	1.2
7H-2, 23.1	51.51	2.8
7H-3, 31.8	53.10	4.9
7H-3, 53.6	53.31	4.7
7H-3, 62.6	53.40	9.6
7H-3, 95.3	53.73	2.9
7H-4, 7.9	54.35	2.9
8H-1, 13.1	59.43	13.7
8H-1, 37.6	59.68	13.5
8H-1, 58.7	59.89	1.1
8H-1, 70.5	60.01	2
8H-2, 35.5	61.15	43.1
8H-2, 88.1	61.67	46.3
8H-3, 62.5	62.91	5.6
8H-3, 124.7	63.54	1.2
8H-4, 21.8	63.99	1.6
8H-4, 43.5	64.21	2.4
8H-4, 83.7	64.61	4.9
8H-4, 128.1	65.06	12
8H-5, 40.4	65.67	24.6
8H-5, 68.5	65.95	1.2
8H-5, 71.0	65.97	1.1
8H-6, 78.2	67.54	1.4
8H-6, 131.3	68.07	5.4

Note: Voids may be curated empty or filled with styrofoam.

Table 2. Depths (mbsf) of tops of sections from Site 893, adjusted by deletion of voids greater than 1 cm.

Section depth	Section depth	Section depth
146-893A-	10H-4, 86.92	19H-6, 175.36
1H-1, 0.00	10H-5, 88.40	19H-CC, 176.65
1H-2, 1.48	10H-6, 89.88	20H-1, 177.50
1H-3, 2.99	10H-7, 90.67	20H-2, 178.84
1H-4, 4.50	10H-CC, 92.14	20H-3, 180.34
1H-5, 5.98	11H-1, 92.00	20H-4, 181.76
1H-CC, 6.24	11H-2, 93.39	20H-5, 183.25
2H-1, 6.50	11H-3, 94.89	20H-6, 184.75
2H-2, 8.00	11H-4, 96.36	20H-7, 186.23
2H-3, 9.44	11H-5, 97.65	20H-CC, 186.76
2H-4, 10.86	11H-6, 98.41	21H-1, 187.00
2H-5, 12.22	11H-CC, 99.88	21H-2, 187.92
2H-6, 13.49	12H-1, 101.50	21H-3, 189.55
2H-7, 14.92	12H-2, 102.83	21H-4, 191.07
2H-CC, 15.70	12H-3, 104.29	21H-5, 192.63
3H-1, 16.00	12H-4, 105.76	21H-6, 194.13
3H-2, 17.47	12H-5, 107.17	21H-CC, 195.24
3H-3, 18.97	12H-6, 107.63	146-893B-
3H-4, 20.41	12H-7, 108.96	1H-1, 0.00
3H-5, 21.85	12H-8, 109.34	1H-2, 1.43
3H-6, 23.21	12H-CC, 110.77	1H-CC, 2.07
3H-7, 24.65	13H-1, 111.00	2H-1, 2.30
3H-CC 34.40	13H-2, 112.16	2H-2, 3.74
4H-1, 25.50	13H-3, 112.36	2H-3, 5.27
4H-2, 26.76	13H-4, 113.77	2H-4, 6.78
4H-3, 28.16	13H-5, 115.09	2H-5, 8.33
4H-4, 29.58	13H-6, 116.58	2H-6, 9.82
4H-5, 30.82	13H-7, 118.06	2H-7, 11.32
4H-6, 32.22	13H-8, 119.55	2H-CC, 11.87
4H-7, 33.65	13H-CC, 120.29	3H-1, 11.80
4H-CC, 34.40	14H-1, 120.50	3H-2, 13.13
5H-1, 35.00	14H-2, 122.02	3H-3, 14.62
5H-2, 36.35	14H-3, 123.56	3H-4, 16.09
5H-3, 37.68	14H-4, 125.05	3H-5, 17.49
5H-4, 39.07	14H-5, 126.53	3H-6*, 18.54
5H-5, 40.41	14H-6, 126.77	3H-7, 19.81
5H-6, 41.86	14H-7, 126.93	3H-CC, 20.60
5H-7, 43.07	14H-8, 128.41	4H-1, 21.30
5H-CC, 43.66	14H-9, 129.87	4H-2, 22.80
6H-1, 44.50	14H-CC, 130.28	4H-3, 24.25
6H-2, 45.64	15H-1, 130.00	4H-4, 25.71
6H-3, 46.90	15H-2, 131.21	4H-5, 27.10
6H-4, 48.24	15H-3, 132.73	4H-6, 28.56
6H-5, 49.67	15H-4, 134.26	4H-7, 29.98
6H-6, 51.13	15H-5, 135.87	4H-CC, 30.73
6H-7, 52.49	15H-6, 137.48	5H-1, 30.83
6H-CC, 53.34	15H-7, 138.97	5H-2, 31.97
7H-1, 54.00	15H-CC, 139.74	5H-3, 33.25
7H-2, 54.05	16H-1, 139.50	5H-4, 34.69
7H-3, 55.11	16H-2, 140.69	5H-5*, 36.00
7H-4, 56.23	16H-3, 142.16	5H-6, 37.36
7H-5, 57.56	16H-4, 143.80	5H-7, 38.73
7H-6, 59.03	16H-5, 145.33	5H-CC, 39.55
7H-7, 60.49	16H-6, 146.85	6H-1, 40.30
7H-8, 61.96	16H-7, 148.33	6H-2, 41.80
7H-CC, 62.79	16H CC, 149.18	6H-3, 43.30
8H-1, 63.50	17H-1, 149.00	6H-4, 44.52
8H-2, 63.65	17H-2, 150.46	6H-5, 45.99
8H-3, 65.08	17H-3, 151.99	6H-6, 47.43
8H-4, 66.07	17H-4, 153.54	6H-7, 48.93
8H-5, 67.22	17H-5, 155.11	6H-CC, 49.69
8H-6, 68.68	17H-6, 156.60	7H-1, 49.80
8H-7, 70.07	17H-7, 158.05	7H-2, 51.28
8H-8, 71.32	17H-CC, 158.43	7H-3, 52.75
8H-CC, 71.96	18H-1, 158.50	7H-4, 54.02
9H-1, 73.00	18H-2, 159.95	7H-5, 55.48
9H-2, 74.25	18H-3, 161.40	7H-6*, 56.97
9H-3, 75.55	18H-4, 162.98	7H-7, 58.13
9H-4, 76.78	18H-5, 164.43	7H-CC, 58.99
9H-5, 78.13	18H-6, 165.88	8H-1, 59.30
9H-6, 79.58	18H-7, 167.32	8H-2, 60.49
9H-7, 79.74	18H-CC, 167.74	8H-3, 61.09
9H-8, 81.12	19H-1, 168.00	8H-4, 62.51
9H-CC, 82.01	19H-2, 169.49	8H-5, 63.77
10H-1, 82.50	19H-3, 170.88	8H-6, 65.00
10H-2, 83.87	19H-4, 172.40	8H-7, 66.42
10H-3, 85.35	19H-5, 173.88	8H-CC, 67.24

Note: 3-cm paleontological whole-round sections taken routinely from core catchers (CC) and 10-cm interstitial-water whole-round sections taken from alternate cores in Hole 893B (marked by an asterisk) are NOT treated as voids in this compilation, although no material remains in liner.

Table 3. Chronology and sedimentation rates in Hole 893A.

Sample/event	Depth at base of interval (mbsf)	Age at base of interval (ka)	Sedimentation rate in interval (mm/yr)
Top of section (?)	−1.21	—	—
5H-7, 11p	43.17	28.896	1.54
Stage 3.3–3.31	73.89	51	1.39
Stage 4.22–4.23	90.49	65	1.19
*	113.89	90	0.94
*	116.35	90	*
Stage 5d/5e	140.69	116	0.94
Stage 5e (5.51)	147.46	122.56	1.03
Termination II	156.87	127	2.12
Stage 6.41	195	161.61	1.10

Notes: Depths are corrected for gas voids (Table 1). ^{14}C data for 16 samples (Ingram and Kennett, this volume) between 3.62 and 43.17 mbsf were fitted with a curve (r^2 = 0.998): age = $a + b$ (depth)^c where a = 0.474657733, b = 527.3684544, and c = 1.059172067. Ages were assigned to depths below 43.17 mbsf by linear interpolation between the ^{18}O and pollen events (Heusser, this volume). For the purposes of this curve fit, zero age was assumed to occur at zero depth. Assuming zero age to occur at −1.21 mbsf in Hole 893A, as suggested by correlation between holes with the color data, the curve parameters were adjusted to be a = 30.08622645, b = 522.3079487, and c = 1.061531766, with r^2 = 0.995. *The interval between 113.89 and 116.35 mbsf consists of a single turbidite layer, presumed to have been deposited instantaneously.

Dartnell (this volume) that variations in paleoproductivity and other carbon measures do not reflect low frequency climatic forcing functions, such as Milankovitch cycles. Schaaf and Thurow (this volume) also saw a correlation with the 86-year secular solar cycle in their gray scale measurements, which they attributed to variations in terrigenous flux rates and in sizes of summer phytoplankton assemblages; however, their data did not show the correlations with the higher-frequency cycles seen in this study.

Core-core Correlation

The upper 50 m of luminance (Y) data from each hole are plotted in Figure 12, where the depth scale for Hole 893A has been shifted to greater depths in the column by 1.21 m to correlate ($r = 0.683$; significant at the 99% confidence level) with the data from Hole 893B. An argument, based on the color data alone, can be made that approximately 1.2 m of material is present at or near the top of the Hole 893B that was not recovered from Hole 893A. Peaks on which this correlation is based are listed in Table 4. Correlated peaks within the upper 10 m of each hole are shown in Figure 13.

Schaaf and Thurow (this volume) reported that 2.9 m of material may be missing from the top of Hole 893A relative to Hole 893B, more than double the 1.2 m observed in this study. Rack and Merrill (this volume) correlated the color data with the magnetic susceptibility data in considerable detail, and conclude that approximately 70 cm is missing from the top of Hole 893A, relative to Hole 893B, that additional material (75 to 100 cm) may be missing from Hole 893A between Cores 1H and 2H, and that between 1.5 and 2.0 m of material may be missing from between Cores 2H and 3H in both holes. Correlation of multiple data sets improves the clarity of the view tremendously.

During the January 1993 splitting party, the scientific party noticed strong similarities in the spacing of fine laminations within intervals between 50 and 53 mbsf in both holes, and proposed that these intervals may be correlative (Kennett, Baldauf, et al., 1994; Figure 12). Close-up photographs of portions of these intervals are shown in Figure 14, together with CIE luminance (Y) data gathered from LEAF high-resolution images which were captured in August 1994, 19 months after the cores had been split and exposed to air. The laminations pictured in figure 11 of the site chapter can still be seen clearly in Figure 14. Linear correlation (r = 0.588; significant at the 99%

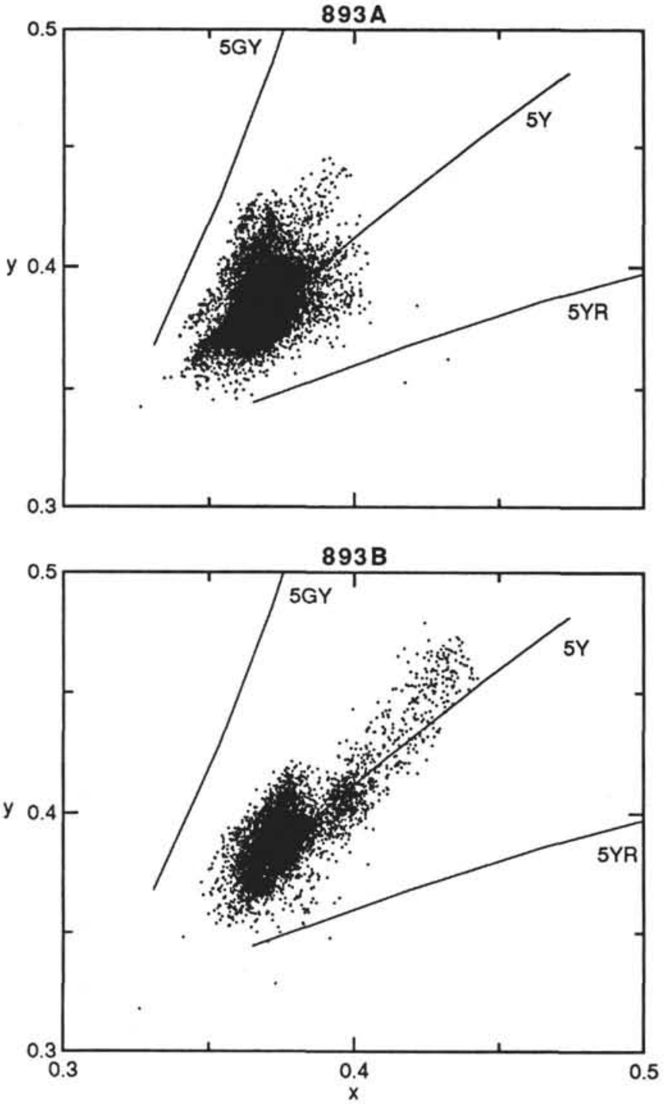

Figure 4. CIE 1931 chromaticity data for Holes 893A and 893B projected into the (x, y) plane of Figure 1. Data points shown are averages that attenuate the data set to one point every 1.25 cm.

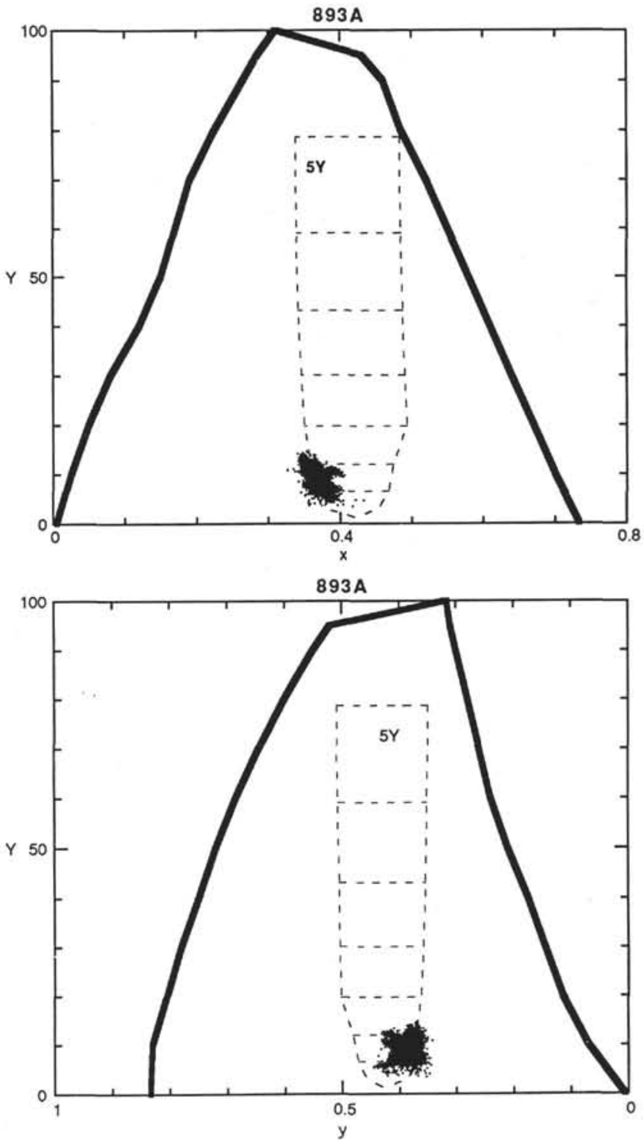

Figure 5. Projection of CIE 1931 CIE chromaticity data (1.25 cm averaged data set) for Hole 893A into (x, Y) and (y, Y) coordinate planes. Heavy line is the projection envelope of the three-dimensional CIE chromaticity space (MacAdam, 1935). Munsell 5Y hue surface is projected as a dashed envelope, with values shown as horizontal dashed lines.

confidence level) between these intervals was achieved by shifting the depth scale of the Hole 893A material relative to that of Hole 893B upward (i.e., to shallower depths) by approximately 0.7 m. This depth shift is more than half the magnitude of and opposite in direction to the shift observed in shallower portions of the cores; however, it is impossible to tell from these data whether the depth difference is due to loss of material during drilling or to differential compaction or erosion. Given the gassy nature of these cores, and the observed losses of material during their opening on the catwalk, it is more likely that this depth difference is caused by drilling problems than by natural phenomena.

CONCLUSIONS

The ODP color digital imaging system is a useful tool for logging color changes in cores as a function of depth, although there remains room for improvement in automation of the data collection and editing processes. The instrument captures and stores images in digital formats that are not subject to the degradation commonly observed in photographic films, so that useful studies of colors, lithologies, structures, textures, bioturbation and other phenomena visible in images of the split-core surface can be conducted long after the original cores have oxidized, faded, and desiccated. Standard image analytical tools, such as ImagePro or NIH Image, can manipulate these images so they form an archive which will have value indefinitely.

The images can be used to map voids in detail, so that depth data for other data sets (MST and discrete sample analyses) can be corrected automatically to eliminate spurious data and so that they can be compared on comparable depth axes. Dense color data sets can be gathered from such images, averaged or smoothed to suit the needs

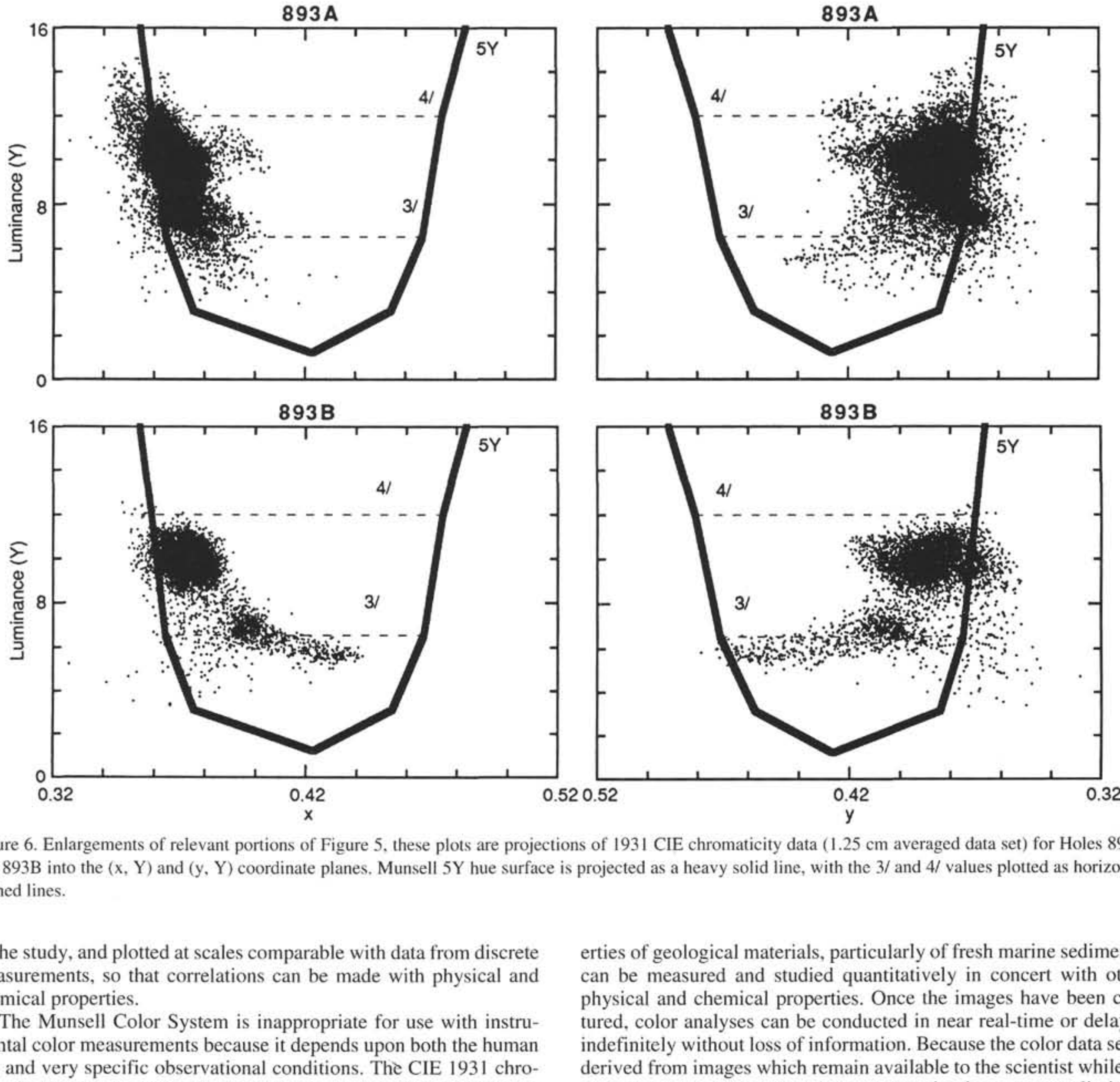

Figure 6. Enlargements of relevant portions of Figure 5, these plots are projections of 1931 CIE chromaticity data (1.25 cm averaged data set) for Holes 893A and 893B into the (x, Y) and (y, Y) coordinate planes. Munsell 5Y hue surface is projected as a heavy solid line, with the 3/ and 4/ values plotted as horizontal dashed lines.

of the study, and plotted at scales comparable with data from discrete measurements, so that correlations can be made with physical and chemical properties.

The Munsell Color System is inappropriate for use with instrumental color measurements because it depends upon both the human eye and very specific observational conditions. The CIE 1931 chromaticity system is a better choice because it was designed for use with instrumental techniques, and because it permits mathematical manipulation of the chromaticity (x, y, Y) data, including statistical and time-series analyses which cannot be performed within the Munsell Color System. Projection of Munsell hue and value boundaries into CIE chromaticity space confirms that the colors measured digitally within a few days of splitting agree closely with the Munsell System colors identified by the sedimentologists who performed the visual descriptions.

Correlation of the color data between Holes 893A and 893B suggests that as much as 1.2 m of material may be present at or near the top of Hole 893B which was not recovered from Hole 893A, and that the intervals between 50 and 53 m thought to be correlative on the basis of visual inspection are in fact correlative. Correlation of the color data with other continuous physical property data sets improves the interpretation of both data sets (e.g., Rack and Merrill, this volume).

Through digital imaging, which can be accomplished with off-the-shelf equipment available for relatively modest cost, color properties of geological materials, particularly of fresh marine sediments, can be measured and studied quantitatively in concert with other physical and chemical properties. Once the images have been captured, color analyses can be conducted in near real-time or delayed indefinitely without loss of information. Because the color data set is derived from images which remain available to the scientist while he or she is processing the data, it becomes a simple process to eliminate artifacts resulting from drilling disturbances, gas voids, or other unnatural disturbances of the split core surface. The density of color measurements is limited only by the scale of the image (e.g., mm^2 of sample per pixel), which is a choice made at the time of image capture; thereafter, measurements can be made as densely as the scientist wishes, including the very high density needed for time-series or statistical manipulations, and then can be decimated as required for comparison with other data sets. Resulting color measurements can be correlated with a variety of other sample, MST, and well-log measurements.

ACKNOWLEDGMENTS

We wish to thank Mr. Bradley Cook, who assisted with collecting the core images. Ms. Randy Merrill has generously spent many long hours pulling the color data out of the images. Without the generous

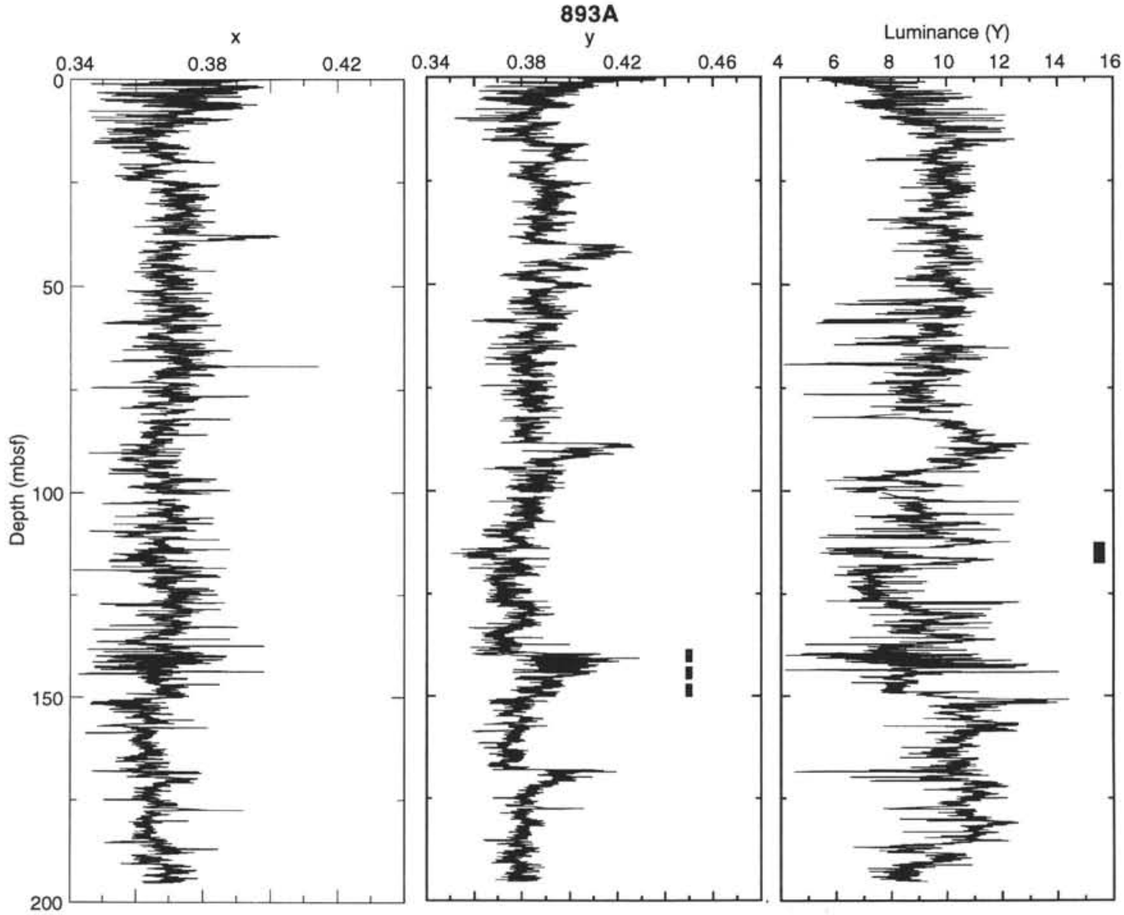

Figure 7. CIE 1931 chromaticity data for Hole 893A (1.25 cm averaged data set) plotted against void-corrected depth (Tables 1, 2). Data have been smoothed with a 5-point running average. Solid vertical bar in luminance plot corresponds to thick turbidite between 113.9 and 116.7 mbsf. Dashed vertical bar in y-chromaticity plot parallels Core 146-893A-16H, which is enlarged in Figure 9.

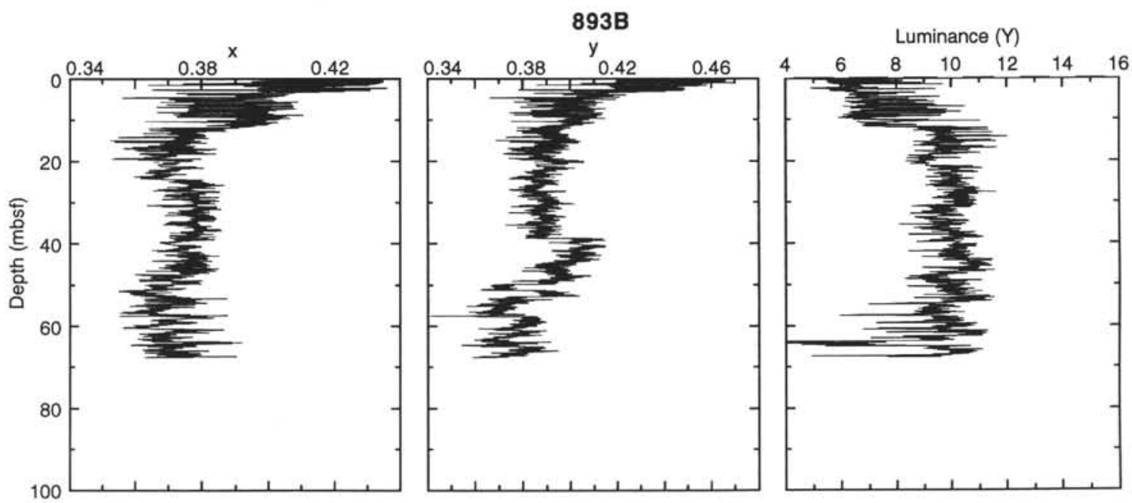

Figure 8. CIE 1931 chromaticity data for Hole 893B (1.25 cm averaged data set) plotted against void-corrected depth (Tables 1, 2). Data have been smoothed with a 5-point running average.

help of these people, this study would not have been possible. We also thank Alan Mix and Michael Schaaf for useful reviews. Financial support for development of the ODP color digital imaging system has been provided by the Ocean Drilling Program of Texas A&M University under Contracts 64–84 and 1–94 with the Joint Oceanographic Institutions, Inc.

REFERENCES

Agoston, G.A., 1987. *Color Theory and its Application in Art and Design* (2nd ed.): Berlin (Springer-Verlag).

Billmeyer, F.W., Jr., and Saltzman, M., 1981. *Principles of Color Technology:* New York (Wiley).

Kennett, J.P., Baldauf, J.G., et al., 1994. *Proc. ODP, Init. Repts.*, 146 (Pt. 2): College Station, TX (Ocean Drilling Program).

Kodak, 1990. *Handbook of Kodak Photographic Filters:* Rochester, NY (Eastman Kodak Co.), Kodak Publ. #B-3.

Landscheidt, T., 1987. Long-range forecasts of solar cycles and climate change. *In* Rampino, M.R., Sanders, J.E., Newman, W.S., Königsson, L.K. (Eds.), *Climate:* New York (Van Nostrand Reinhold).

MacAdam, D.L., 1935. Maximum visual efficiency of colored materials. *J. Opt. Soc. Am.*, 25:361–367.

Mix, A.C., Harris, S.E., and Janecek, T.R., 1995. Estimating lithology from noninclusive reflectance spectra: Leg 138. *In* Pisias, N.G., Mayer, L.A., Janecek, T.R., Palmer-Julson, A., and van Andel, T.H. (Eds.), *Proc. ODP, Sci. Results,* 138: College Station, TX (Ocean Drilling Program), 413–427.

Mix, A.C., Rugh, W., Pisias, N.G., Veirs, S., Leg 138 Shipboard Sedimentologists (Hagelberg, T., Hovan, S., Kemp, A., Leinen, M., Levitan, M., Ravelo, C.), and Leg 138 Scientific Party, 1992. Color reflectance spectroscopy: a tool for rapid characterization of deep-sea sediments. *In* Mayer, L., Pisias, N., Janecek, T., et al., *Proc. ODP, Init. Repts.*, 138 (Pt. 1): College Station, TX (Ocean Drilling Program), 67–77.

Munsell, A.H., 1929. *Munsell Book of Color:* Baltimore (Munsell Color Co.).

———, 1963. *A Color Notation:* Baltimore (Munsell Color Co.).

Newhall, S.M., Nickerson, D., and Judd, D.B., 1943. Final report of the O.S.A. Subcommittee on the spacing of the Munsell Colors. *J. Opt. Soc. Am.*, 33:385–418.

Rack, F.R., Gardner, J.V., Merrill, R.B., and Heise, E.A., 1994. Proxy records of Quaternary climate change from the Santa Barbara Basin: Ocean Drilling Program Site 893. *Am. Geophys. Union, Spring Meet., Baltimore.* (Abstract)

Rack, F.R., Heise, E.R., and Merrill, R.B., 1993. Continuous logs of magnetic susceptibility and color reflectance in Late Quaternary sediment cores from the Santa Barbara Basin. *Am. Geophys. Union, Fall Meet., San Francisco.* (Abstract)

Rea, D.K., Basov, I.A., Janecek, T.R., Palmer-Julson, A., et al., 1993. *Proc. ODP, Init. Repts.*, 145: College Station, TX (Ocean Drilling Program).

Rogers, D.F., 1985. *Procedural Elements for Computer Graphics:* New York (McGraw-Hill).

Schaaf, M., and Thurow, J., in press. A fast and easy method to derive highest-resolution time-series-datasets from drill cores and rock samples. *Sediment. Geol.*

Wyszecki, G., and Stiles, W.S., 1982. *Color Science: Concepts and Methods, Quantitative Data and Formulae* (2nd ed.): New York (Wiley).

Date of initial receipt: 31 August 1994
Date of acceptance: 7 April 1995
Ms 146SR-285

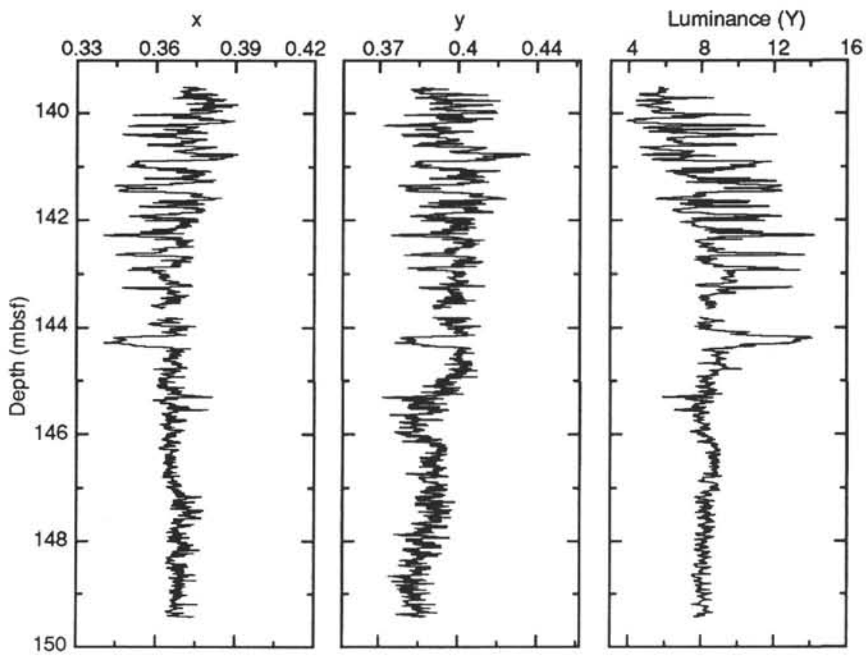

Figure 9. CIE 1931 chromaticity (x, y, Y) data from Core 146-893A-16H, plotted at one point per 0.5 cm, and smoothed with a 5-point running average.

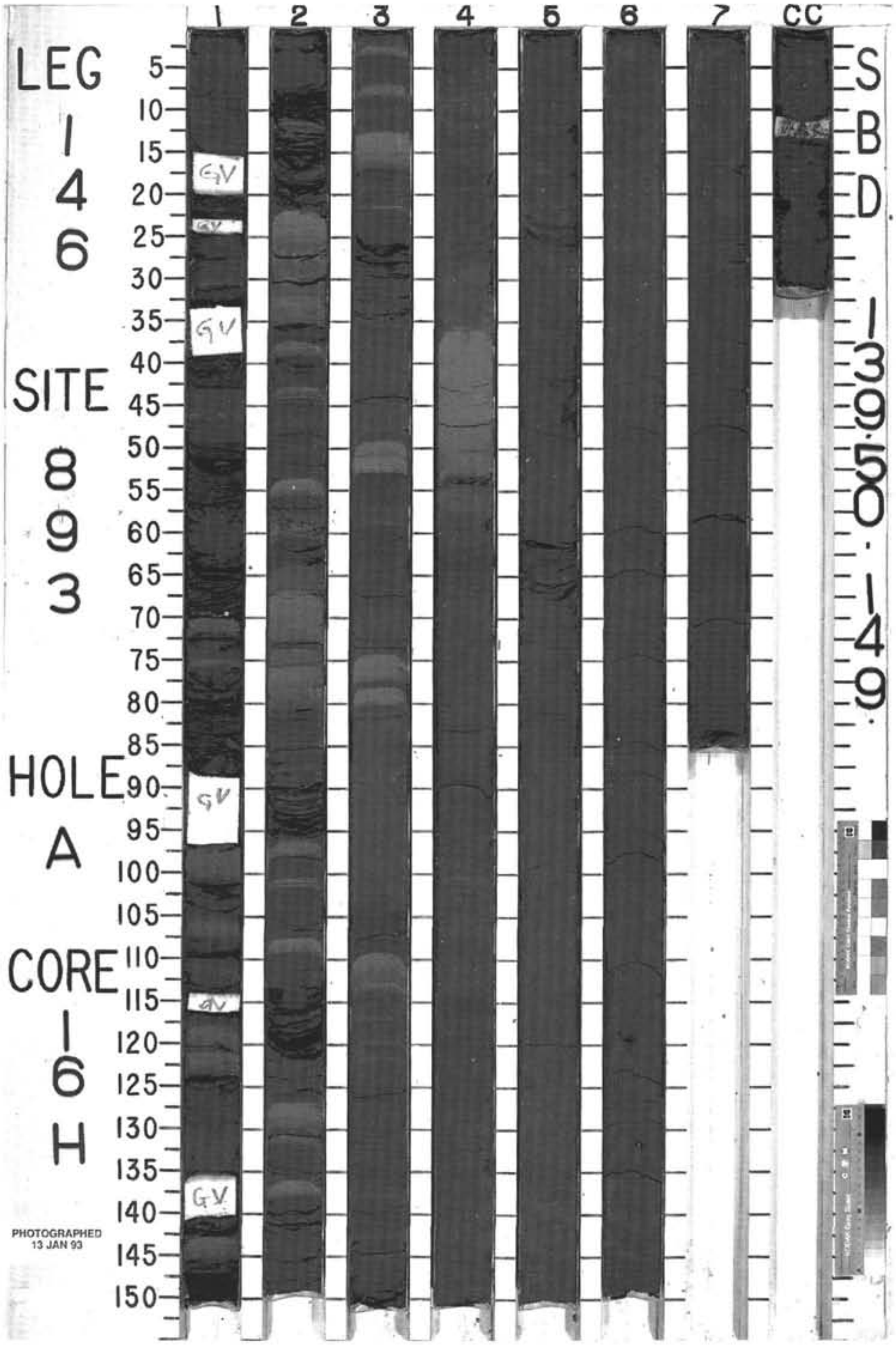

Figure 10. Archival photograph of Core 146-893A-16H. Note the intercalated beds of dark and light olive gray clay visible in the upper three sections, and the more massive clay beds in Section 5 and below. The lithologic variations are clearly visible in the color data plotted in Figure 9, with light gray beds corresponding to positive digressions in Y and to negative digressions in x and y values.

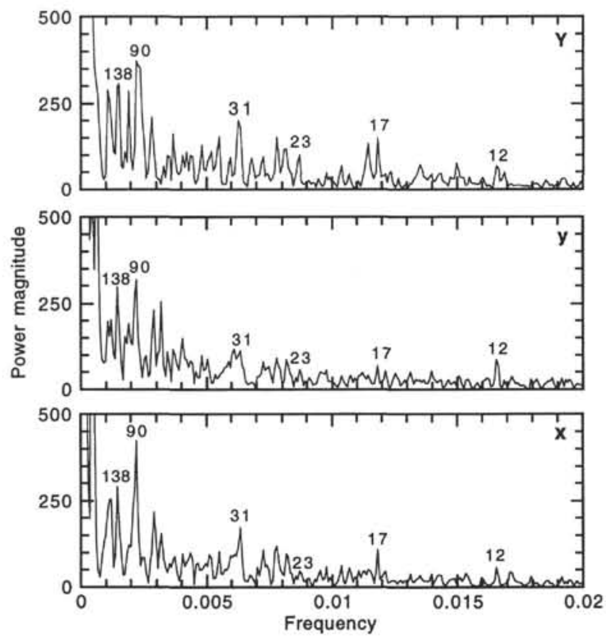

Figure 11. Power spectra of CIE chromaticity data for Cores 146-893A-1H through -5H, which cover the last 30 ka. Sample interval is 0.2 year, so Nyquist frequency is 2.5 cycles/year. Prominent peaks are denoted with periodicity in years.

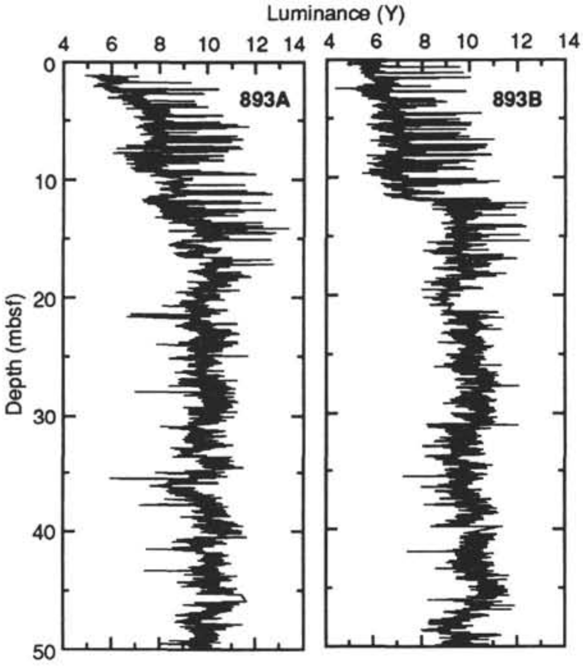

Figure 12. Correlation between luminance (Y) data from the upper 50 m sections of Holes 893A and 893B. Depths of peaks from Hole 893A were linearly correlated with those of Hole 893B using Analyseries (provided by L. Labeyrie). 4357 data points were used from each hole, smoothed with a 5-point running average to reduce the impact of minor events. Resulting correlation coefficient (r) is 0.683. Correlation peak picks are detailed in Table 4 and Figure 13.

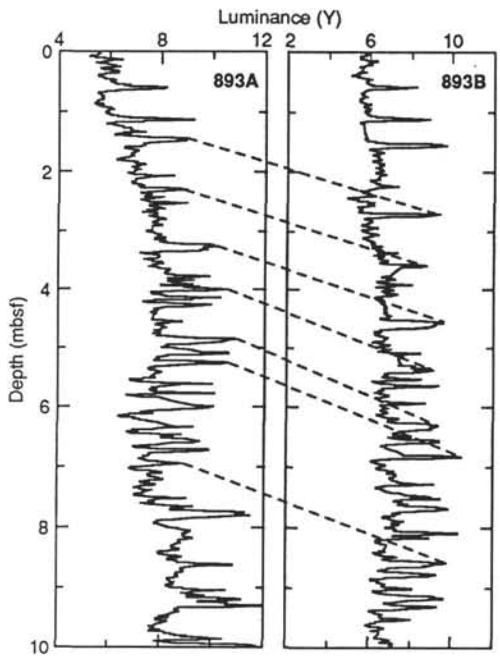

Figure 13. Luminance (Y) peaks correlated between holes in the upper 10 m of Holes 893A and 893B, plotted at original depth, prior to correlation. See Table 4 for precise depths of peaks correlated, and Figure 12 for a plot of the upper 50 m, after correlation. Dashed straight lines connect pairs of peaks used in the linear correlation. A shift of 1.2 m applied to depths in Hole 893A is required to correlate these peaks.

Table 4. Depths (mbsf) correlated between Holes 893A and 893B in Figures 12 and 13.

893A	893B
1.4903	2.7206
2.3015	3.6054
3.2657	4.5567
4.0025	5.3914
4.839	6.2828
5.2555	6.8395
6.951	8.5781
9.9766	11.969
12.314	14.144
17.663	19.401
34.412	35.486
42.007	43.343

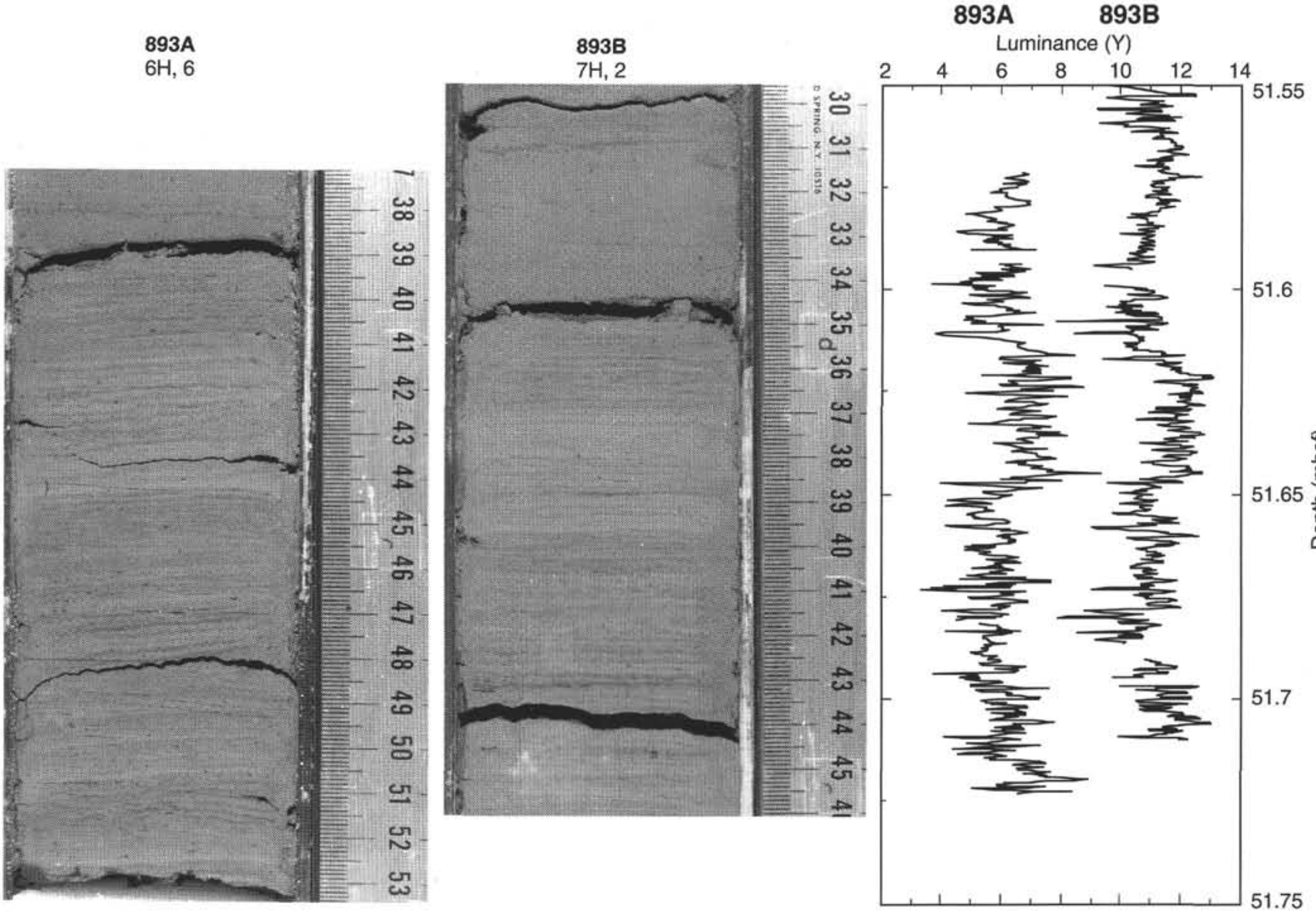

Figure 14. Images and high-resolution CIE 1931 luminance (Y) data from interval 146-893A-6H-6, 37.1–53.4 cm, correlated with those from interval 146-893B-7H-2, 29.6–46.1 cm. These images were captured in color (2048 × 2048 × 42-bit pixels) with the LEAF digital camera back. The unsmoothed luminance data shown on the right were taken from color versions of the images printed on the left. These intervals are part of the finely laminated portions of Subunit 1C for which the scientific party proposed correlation on the basis of visual similarity (Kennett, Baldauf, et al., 1994, figure 11, p. 30). To accomplish the correlation, Hole 893A depth values have had to be shifted upward in the column by 0.707 m ± 0.0018 m, resulting in a correlation coefficient of 0.588 between the two data sets (690 points each). Measured luminance values from Hole 893A have been offset (by –5) in this figure to facilitate comparison with the Hole 893B data.